Evolution of Specific Heat Capacity with Temperature for Typical Supports Used for Heterogeneous Catalysts

Authors:

Xiaojia Lu, Yanjun Wang, Lionel Estel, Narendra Kumar, Henrik Grénman, Sébastien Leveneur

Date Submitted: 2020-12-17

Keywords: micro-calorimeter C80, heterogeneous catalytic material, specific heat capacity

Abstract:

Heterogeneous catalysts are widely used in the chemical industry. Compared with homogeneous catalysts, they can be easily separated from the reaction mixture. To design and optimize an efficient and safe chemical process one needs to calculate the energy balance, implying the need for knowledge of the catalyst's specific heat capacity. Such values are typically not reported in the literature, especially not the temperature dependence. To fill this gap in knowledge, the specific heat capacities of commonly utilized heterogeneous catalytic supports were measured at different temperatures in a Tian?Calvet calorimeter. The following materials were tested: activated carbon, aluminum oxide, amberlite IR120 (H-form), H-Beta-25, H-Beta-38, H-Y-60, H-ZSM-5-23, H-ZSM-5-280, silicon dioxide, titanium dioxide, and zeolite 13X. Polynomial expressions were successfully fitted to the experimental data.

Record Type: Published Article

Submitted To: LAPSE (Living Archive for Process Systems Engineering)

Citation (overall record, always the latest version):	LAPSE:2020.1185
Citation (this specific file, latest version):	LAPSE:2020.1185-1
Citation (this specific file, this version):	LAPSE:2020.1185-1v1

DOI of Published Version: https://doi.org/10.3390/pr8080911

processes

MDPI

Article

Evolution of Specific Heat Capacity with Temperature for Typical Supports Used for Heterogeneous Catalysts

Xiaojia Lu [1,2], Yanjun Wang [1], Lionel Estel [1], Narendra Kumar [2], Henrik Grénman [2,*] and Sébastien Leveneur [1,*]

1 Normandie Univ, INSA Rouen, UNIROUEN, LSPC, EA4704, 76000 Rouen, France; xiaojia.lu@insa-rouen.fr (X.L.); yanjun.wang@insa-rouen.fr (Y.W.); lionel.estel@insa-rouen.fr (L.E.)

2 Laboratory of Industrial Chemistry and Reaction Engineering, Johan Gadolin Process Chemistry Centre, Åbo Akademi University, Biskopsgatan 8, FI-20500 Åbo/Turku, Finland; narendra.kumar@abo.fi

* Correspondence: henrik.grenman@abo.fi (H.G.); sebastien.leveneur@insa-rouen.fr (S.L.); Tel.: +33-2329-566-54 (S.L.)

Received: 25 June 2020; Accepted: 20 July 2020; Published: 1 August 2020

Abstract: Heterogeneous catalysts are widely used in the chemical industry. Compared with homogeneous catalysts, they can be easily separated from the reaction mixture. To design and optimize an efficient and safe chemical process one needs to calculate the energy balance, implying the need for knowledge of the catalyst's specific heat capacity. Such values are typically not reported in the literature, especially not the temperature dependence. To fill this gap in knowledge, the specific heat capacities of commonly utilized heterogeneous catalytic supports were measured at different temperatures in a Tian–Calvet calorimeter. The following materials were tested: activated carbon, aluminum oxide, amberlite IR120 (H-form), H-Beta-25, H-Beta-38, H-Y-60, H-ZSM-5-23, H-ZSM-5-280, silicon dioxide, titanium dioxide, and zeolite 13X. Polynomial expressions were successfully fitted to the experimental data.

Keywords: specific heat capacity; heterogeneous catalytic material; micro-calorimeter C80

1. Introduction

Catalysts play a crucial role in the modern chemical industry, and indirectly the development of society. According to statistics, there are around 30,000 different raw materials and chemical intermediates that are synthesized by using catalysts. These materials are not only related to people's food, clothing, and housing, but also involve modern high-tech fields such as information transmission, network technology, aerospace [1–3], and bioengineering [4,5]. Today, researchers are committed to developing more efficient, selective, less expensive, and greener industrial catalysts in order to upgrade current chemical production technologies.

Heterogeneous catalysts are the most widely used catalysts in industrial production, due to their versatile physicochemical properties, high hydrothermal stability, and efficient catalyst recovery/reusability [6,7]. Indeed, heterogeneous catalysis contributes to about 90% of chemical production processes and to more than 20% of all industrial products [8]. There are numerous types of catalytic materials and supports, among which zeolite, mesoporous catalyst, resin catalyst, alumina, and activated-carbon-based catalysts are typically used in industry. Usually, the characteristics of a catalyst, such as specific surface area, particle size, morphology, porosity, and acidity, are determined, as they are crucial parameters for performance and use in industrial applications. However, the effect of the heat capacity of catalysts on large-scale chemical processes has not received much attention in the literature, even though the thermodynamic properties vary significantly between different catalysts

or catalyst supports. Industrial processes can be performed under non-isothermal conditions with different types of catalysts and catalyst loadings, and many processes are performed in continuous reactors with high catalyst loads. Determining the thermal properties of a catalyst is necessary when evaluating the thermal risk of a process performed under non-isothermal conditions, especially when considering larger-scale production. Besides risk assessment, the heat capacity of the catalyst can influence the operation and temperature profile of a reactor significantly. This issue often arises at the start of a process. The heat capacity of a large catalyst bed can have a significant impact on the energy balance. These aspects can be very important for robust modeling and simulation purposes, which are the basis of the reliable design and operation of chemical processes. However, much attention has typically been focused on determining the physical properties of the bulk phase [9–11] in detail, including heat capacity, while very little data are found for heterogeneous catalysts [12,13].

Differential scanning calorimetry (DSC) [14] is a conventional method for measuring a variety of thermodynamic properties. It has been widely applied to the specific heat capacity (C_p) measurement of different materials, such as frying oil [15], alloys [16], phase change materials [17], and solid lead [18]. However, the sensitivity of measuring and calculating specific heat capacity by general DSC is usually very low, resulting in a relative error of 5–10%, mainly due to the weak baseline reproducibility. In addition, poor correction accuracy is obtained by this method. The calibration of general DSC instruments is usually performed by melting the standard metal, and it is greatly affected by the sample morphology, reaction type, and atmosphere. Moreover, sample adaptability is very poor. The sample is always required to maintain good contact with the bottom of the crucible to ensure excellent heat conduction; thus, the C_p test of powders and large heterogeneous samples is greatly restricted. Furthermore, liquid samples are also not applicable, as small crucibles (<100 μL) are usually used, which are difficult to seal.

The Setaram C80 3D Calvet Calorimeter is powerful and flexible. Measurement by C80 is similar to DSC, i.e., the energy difference between the measured substance and the reference substance is determined under a programmed-temperature control. However, the Calvet calorimeter possesses a caloric efficiency of up to 94%, whereas that of typical plate DSC is between 20 and 40%. Besides this, the detector adopts a three-dimensional full-clad calorimetric method, and, contrary to the general DSC, it takes into account the heat flow that may occur inside the sample itself during calorimetry. The C80 measurement is independent of the weight, form, and nature of the sample, the type of cell utilized, the manner of contact between sample and sensor, and the nature of the sweeping gas (inert, oxidizing, wet, etc.), providing an excellent precision, even for samples with irregular shapes or uneven heat conduction. Furthermore, the temperature is raised and lowered at a very consistent, slow rate, which makes the C_p measurement more accurate. The C80 calorimeter has found an application in the precise determination of heat capacities of different materials [19–23].

In this work, a micro-calorimeter (C80) was for the first time applied for determining the specific heat capacity of commonly used catalytic materials/supports as a function of temperature. These data contribute to filling an important gap in knowledge in this area. The data can be used to estimate the kinetic constants and reaction enthalpies of chemical processes at both laboratory and industrial scale. Moreover, the heat capacities are important basic data for safety and risk assessment purposes.

2. Materials and Methods

2.1. Calorimetric Reactor Rystem

The C80 Tian–Calvet calorimeter (Figure 1), manufactured by Setaram instrumentation, has absolute calibration, featuring a three-dimensional transducer with maximum sensitivity. Its measuring temperature range is between ambient (298 K) and 573 K. The apparatus is equipped with twin detectors and twin cells (a measurement cell and a reference cell), which are surrounded by thermocouples. External thermal interferences in the calorimetric system, such as phi-factor [24], are eliminated by a differential coupling of the measurement and reference detectors, allowing for

determination of the heat flow for radiation, convection, and conduction in a very precise way. The standard error of the temperature measurement is 0.1 K, and the standard error of enthalpy measurement is 0.1%. The C80 calorimeter has been successfully applied previously in studying different processes, such as hydration, dehydration, denaturation, dissolution, gas adsorption, phase transition, and monomer polymerization. Moreover, the C80 is operated by Setsoft 2000 (Setaram thermal analysis software), and heat measurement can be carried out under an isothermal mode or a temperature-programmed mode, which makes it an ideal device for the measurement of C_p.

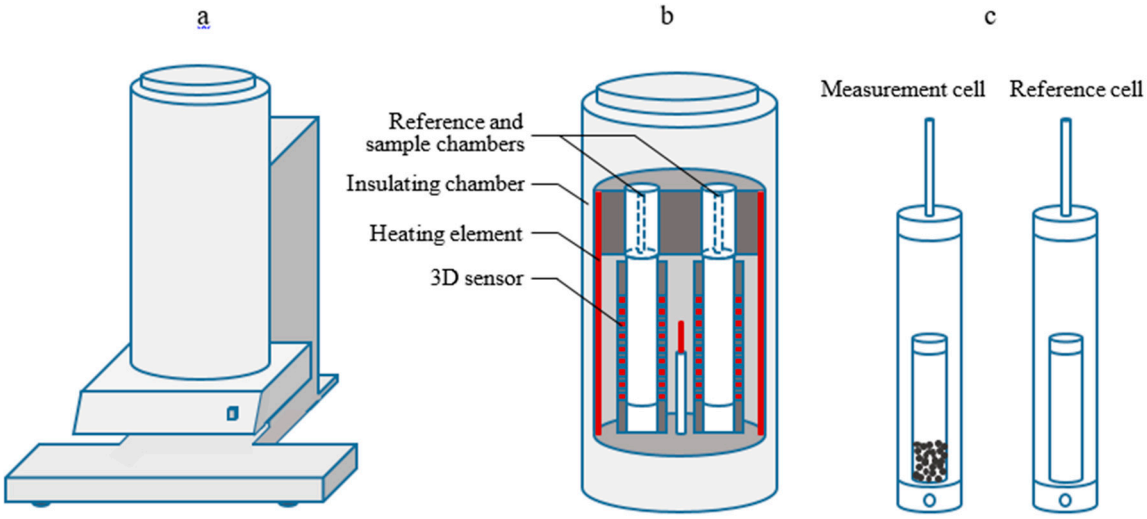

Figure 1. (**a**) General view of the C80 micro-calorimeter from Setaram; (**b**) the heating block showing the geometry for the reference and measurement cells; (**c**) the Hastelloy reversing mixing cells utilized in the current work and their contents.

The current study employed a C80 micro-calorimeter for the measurement of the specific heat capacity of different catalytic materials, in the temperature range 313–453 K. In order to determine the heat flow (energy absorbed by the samples) at different temperatures, a pair of Hastelloy reversing mixing cells was employed. In the C80, the heat flow determined is proportional to the C_p value. Hence, the heat capacity is calculated directly from the heat flow signal. The isothermal baselines before and after each temperature rise need to be long enough for the system to stabilize and reach stationary conditions. The accuracy of the instrument was successfully verified by sodium chloride before the formal test.

The samples were dried overnight in an oven at 393 K before the measurement. The measurement cell was filled with a known amount (0.5–3.1 g) of sample, while the reference cell was kept empty, as shown in Figure 1. The calorimeter was sealed, and the heating was started according to the following temperature program: After reaching the first set point (313 K), the two cells were left to stabilize for 8400 s before increasing the temperature by 2 K at a speed of 0.5 K/min. During the heating process, the variation of heat flow was recorded by the Setsoft 2000 software. The system was then kept at a constant temperature for 4200 s, followed by being heated to the next set point (333 K) at a speed of 1 K/min, and then stabilized for 8400 s. These steps were repeated multiple times with regular intervals until the last heat flow peak (at 453 K) was gained.

The specific heat capacity measurement was repeated three times for each catalytic material and was done with the same, single sample, giving a maximum standard error of 1.79%, which demonstrated excellent repeatability and the absolute accuracy of the C80.

In order to evaluate the standard deviation of the heat capacity measurement, Equation (1) was employed.

$$s(C_p) = \sqrt{\frac{\sum_{i=1}^{n} \left(C_{pi} - \overline{C_p}\right)^2}{n-1}} \quad (1)$$

where C_{pi} is the experimental value of the specific heat capacity of the *i*th measurement, $\overline{C_p}$ is the arithmetic mean value of the specific heat capacity of the n experimental results considered, and n is the number of times the experiment was repeated for a catalytic material at each temperature, which was 3 in the current work.

Figure 2 shows an example of the evolution of heat flow and temperature at a set point (333 K) in a series measurement, where the heat flow curves represent the difference in heat flow between the measurement cell and the reference cell in the presence and absence of the sample. The difference between the enthalpies of the two cells, i.e., the energy absorbed by the sample, was determined by directly integrating the heat flow peak of the sample (blue). The data were corrected by subtracting the corresponding blank (red) curve. The corrected data were subsequently used to calculate the C_p value of the sample, using Equation (2).

$$C_p = \frac{Q_c - Q_b}{m \times \Delta T} \tag{2}$$

in which Q_c and Q_b are the total heat absorbed in the presence and absence of a sample, respectively, m is the mass of the sample placed into the measurement cell, and ΔT is the temperature difference before and after heat capacity measurement at a certain set point, which was around 2 K. A similar approach was used in previous articles published by our group [25,26].

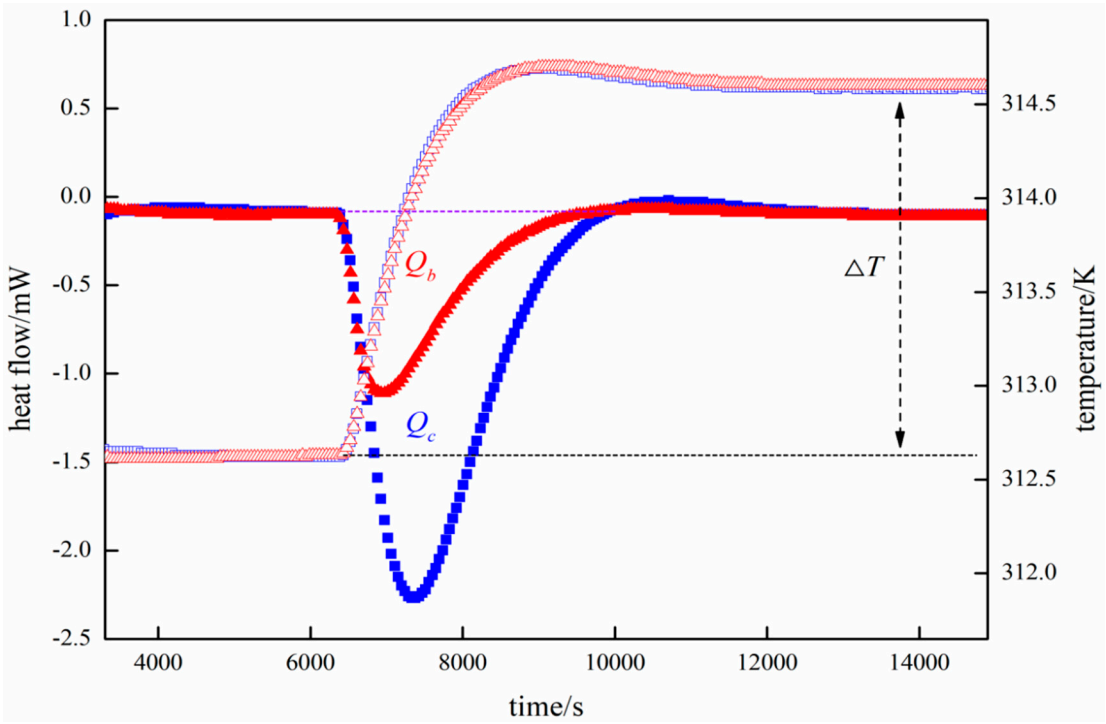

Figure 2. Illustration of C_p measurement with the C80 for a catalytic material. ■, heat flow_H-ZSM-5-23; ▲, heat flow_blank; □, temperature_H-ZSM-5-23; △, temperature_blank.

2.2. Materials

The majority of a catalyst's heat capacity depends on the support, because it is the main constituent of the catalyst. In this study, 11 materials typically used as supports in catalyst preparation were chosen for the precise quantification of C_p values, as listed in Tables 1 and 2. All materials were received or synthesized with high purities (≥99%), and were used without further purification.

Table 1. Type, Physical Form, Molar Ratio of SiO_2/Al_2O_3, and Manufacturer of Catalytic Materials Studied in This Work.

	Type	Physical Form	SiO_2/Al_2O_3 (mol/mol)	Manufacturer
Activated carbon	activated carbon	powder	-	Chemviron
Al_2O_3	aluminum oxide	powder	-	Acros Organics
Amberlite IR120, H-form(53.0–58.0% moisture)	Ion-exchange resin	bead	-	Acros Organics
H-Beta-25	zeolite	powder	25	Zeolyst International
H-Beta-38	zeolite	powder	38	Zeolyst International
H-Y-60	zeolite	powder	60	Alfa Aesar
H-ZSM-5-23	zeolite	powder	23	Zeolyst International
H-ZSM-5-280	zeolite	powder	280	Zeolyst International
SiO_2	silicon dioxide	powder	-	Merck
TiO_2	titanium dioxide	pellet	-	Degussa
Zeolite 13X	zeolite	powder	1.8	Fluka

Table 2. Loading [a] (m) of Catalytic Materials and Temperature Range [b] (T) of C_p Measurement for Each Material.

	m/g	T/K
Activated carbon	0.98	313–453
Al_2O_3	2.00	313–453
Amberlite IR120, H-form	1.95	313–363
H-Beta-25	0.48	313–453
H-Beta-38	1.28	313–453
H-Y-60	0.65	313–453
H-ZSM-5-23	1.09	313–453
H-ZSM-5-280	1.55	313–453
SiO_2	1.37	313–453
TiO_2	3.09	313–453
Zeolite 13X	1.41	313–453

[a] Standard error of mass for specific heat capacity measurement is $u(m) = 0.0001$ g. [b] Standard error of temperature for specific heat capacity measurement is $u(T) = 0.1$ K.

The measurements of a series were taken directly and consecutively at regular intervals, and the measurement for each sample was repeated three times in order to evaluate repeatability. Table 1 shows the basic information of the catalytic materials, and Table 2 displays the loading amount and the temperature ranges for the C_p measurement of each material.

3. Results and Discussion

Specific Heat Capacity Calculation

Eleven commonly utilized catalytic materials, ranging from gel-type anion exchange resins to pure alumina, were studied in a wide temperature range (313–453 K), and the results are shown in Table 3. The data show excellent repeatability of the measurements, as a relatively low combined expanded uncertainty value ($U(C_p) = 31.50$ J·kg^{-1}·K^{-1}, 0.95 level of confidence) was observed.

Table 3. Average Values of Specific Heat Capacity (C_p) of Catalytic Materials as a Function of Temperature (T) [a].

T/K	C_p [b]/(J·kg^{-1}·K^{-1})	T/K	C_p/(J·kg^{-1}·K^{-1})	T/K	C_p/(J·kg^{-1}·K^{-1})
			Activated carbon		
313.59	997.75	382.88	1241.17	422.42	1440.42
333.36	1037.55	392.74	1288.34	432.34	1459.99
353.13	1091.18	402.60	1355.75	442.21	1493.63
372.96	1179.32	412.49	1413.87	452.10	1506.95
			Al_2O_3		
313.57	857.01	382.84	980.10	422.40	1041.78
333.36	903.54	392.73	1003.09	432.31	1052.30
353.15	940.53	402.62	1015.48	442.22	1070.46
372.93	970.32	412.51	1033.37	452.10	1083.82
			Amberlite IR120, H-form		
313.60	1170.74	333.40	1244.29	353.21	1325.63
323.50	1208.66	343.31	1285.37	363.09	1361.98
			H-Beta-25		
313.62	1048.08	382.91	1326.90	422.47	1526.61
333.41	1135.92	392.78	1360.29	432.38	1577.30
353.20	1200.45	402.67	1419.67	442.25	1611.05
373.01	1259.04	412.56	1476.82	452.14	1647.16
			H-Beta-38		
313.63	1361.17	382.93	1632.81	422.50	1896.06
333.42	1428.30	392.81	1685.38	432.41	1983.12
353.22	1499.17	402.70	1757.74	442.28	2090.75
373.03	1575.57	412.59	1819.02	452.17	2201.44
			H-Y-60		
313.59	895.66	382.86	1041.12	422.46	1137.74
333.38	935.65	392.75	1061.84	432.34	1160.56
353.18	979.14	402.64	1085.68	442.22	1184.64
372.97	1019.52	412.55	1110.76	452.12	1209.15
			H-ZSM-5-23		
313.60	1027.35	382.87	1167.70	422.44	1277.33
333.39	1063.39	392.77	1194.68	432.36	1313.73
353.18	1098.71	402.65	1219.61	442.25	1353.51
372.97	1143.54	412.54	1246.26	452.13	1392.11
			H-ZSM-5-280		
313.62	828.34	382.90	896.44	422.47	944.23
333.41	864.92	392.79	910.64	432.38	956.91
353.21	865.08	402.68	927.66	442.26	975.72
373.00	882.80	412.58	940.17	452.15	976.01
			SiO_2		
313.59	1045.04	382.85	1333.53	422.43	1629.69
333.38	1112.58	392.75	1399.71	432.34	1727.41
353.15	1163.06	402.65	1465.91	442.21	1836.38
372.95	1277.84	412.54	1560.48	452.10	1939.65
			TiO_2		
313.61	702.41	382.88	773.06	422.45	796.51
333.40	725.88	392.77	780.21	432.35	805.09
353.20	746.42	402.66	788.29	442.24	813.76
372.99	757.83	412.57	793.80	452.13	818.09
			Zeolite 13X		
313.61	1004.46	382.89	1110.27	422.48	1149.40
333.41	1043.91	392.77	1114.40	432.37	1173.65
353.20	1072.98	402.67	1128.13	442.25	1174.02
373.00	1097.44	412.58	1136.84	452.14	1185.55

[a] Standard error of temperature for specific heat capacity measurement is $u(T)$ = 0.1 K. [b] Combined expanded uncertainty for specific heat capacity is $U(C_p)$ = 31.50 J·kg^{-1}·K^{-1} (0.95 level of confidence).

Figure 3a,b display the C_p values of the materials as a function of temperature. It is clear that the heat capacities of different catalytic materials at the same temperature are not similar, which significantly influences operation under non-isothermal conditions.

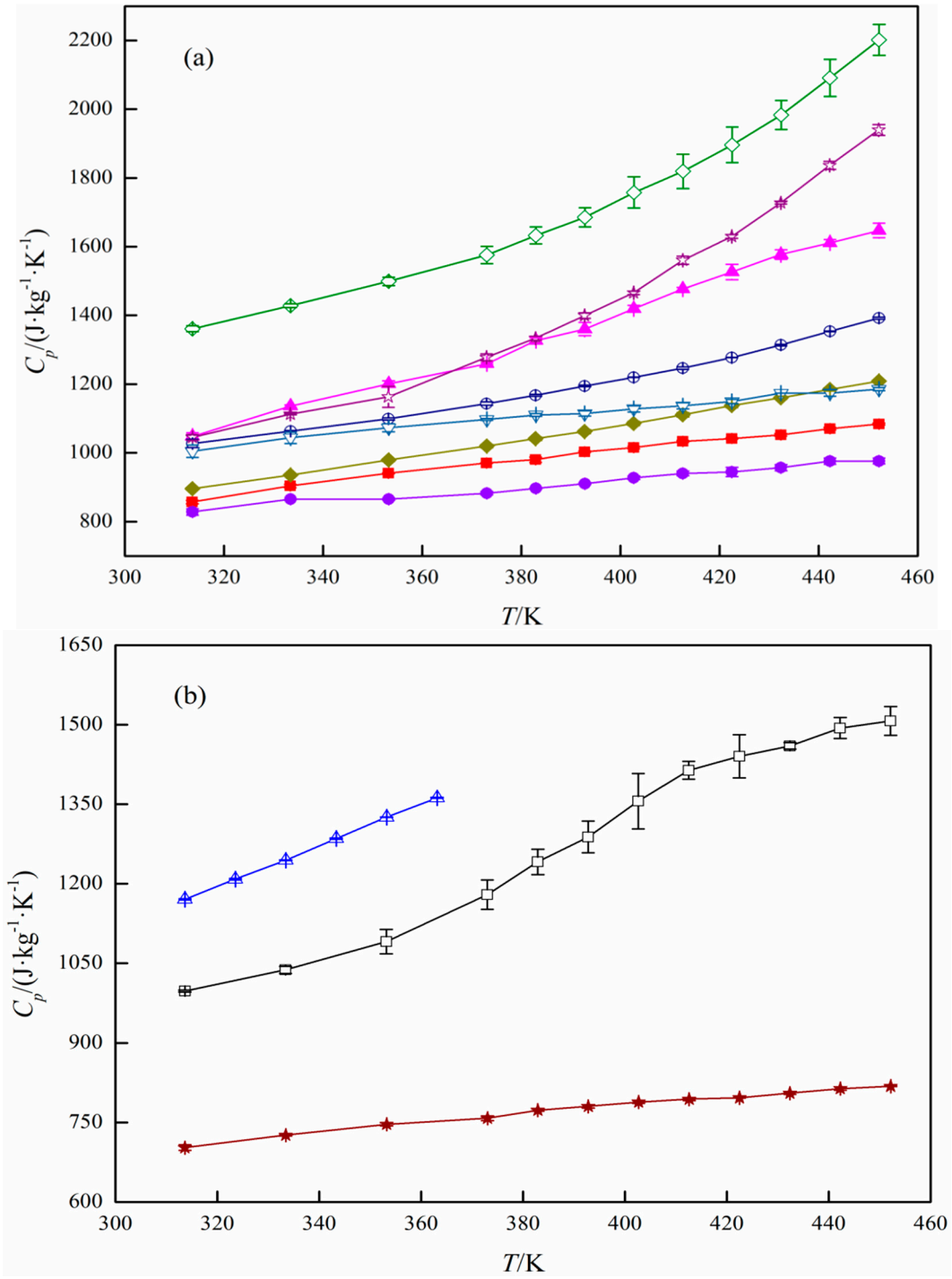

Figure 3. C_p values of (**a**) catalytic materials containing alumina or silica, and (**b**) other catalytic materials as a function of temperature. □, activated carbon; ■, Al_2O_3; △, amberlite IR120, H-form; ▲, H-Beta-25; ◇, H-Beta-38; ◆ , H-Y-60; ○, H-ZSM-5-23; ●, H-ZSM-5-280; ☆, SiO_2; ★, TiO_2; ▽, zeolite 13X.

One can observe that the specific heat capacity of the selected catalytic materials does not have the same behavior as a function of temperature. In general, when the temperature increases, the specific heat capacity increases.

The specific heat capacities of alumina silicate materials are influenced by both the silica and alumina. There is not a clear relationship between the C_p of these materials and the SiO_2/Al_2O_3 ratio. One can notice that the C_p values of H-Beta-38 and SiO_2 are more sensitive to temperature compared with the other materials (Figure 3). The C_p values of TiO_2 are almost independent of temperature.

The obtained C_p values were compared with previously published data [27], as plotted in Figure 4. The C_p values obtained for both activated carbon and alumina are higher than those reported in the literature, even though the curves of the experimental value and the corresponding reference value seem to be parallel to each other. This may be due to the use of different instruments and their related measurement mechanisms. However, a very significant difference in C_p values was obtained for activated carbon and graphite, which are chemically very similar. This was probably caused by the different crystal morphology of these two materials, but not structurally caused, because activated carbon has high porosity. However, further studies are needed to explore the influence of different factors on the heat capacity of these catalytic materials, such as crystallinity, specific surface area, and pore size distribution.

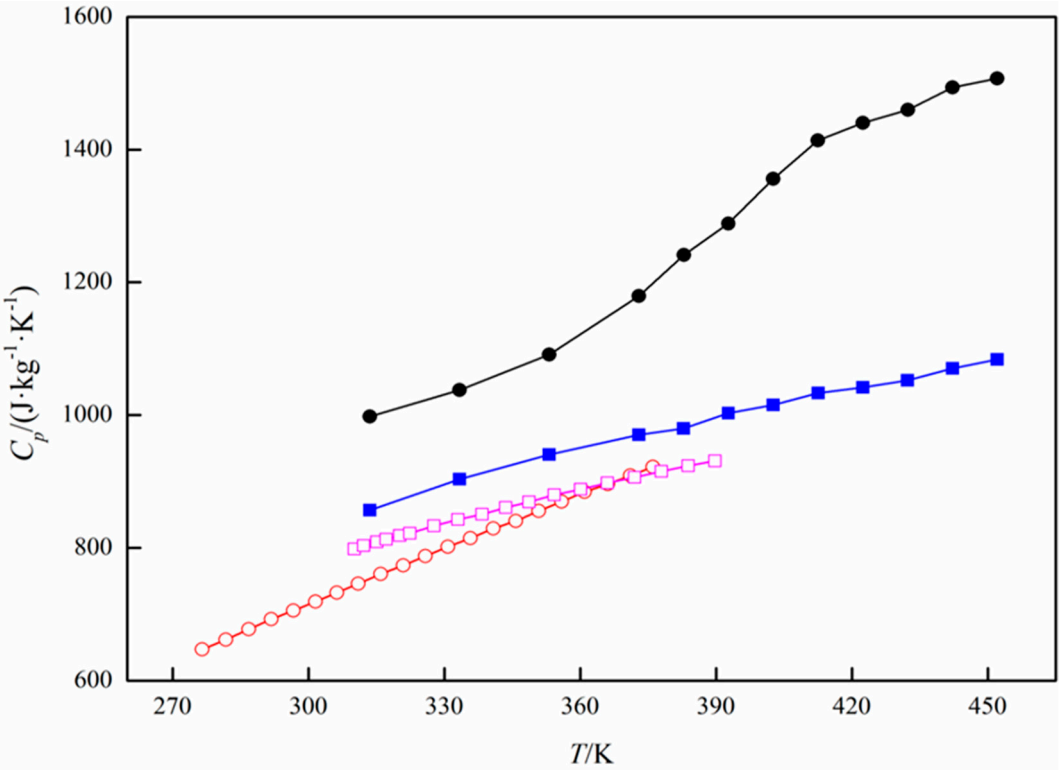

Figure 4. Comparison of C_p values between the current work and references. •, activated carbon_exp; o, graphite_ref. [27]; ■, Al_2O_3_exp; □, Al_2O_3_ref. [27].

Based on the literature [25,26,28], the evolution of C_p with temperature follows a polynomial dependence of the second order. The experimental data in this study were correlated with Equation (3). The fitting parameters, as well as the coefficient of determination (R^2), are given in Table 4.

$$C_p(T) = C_p(T_{ref}) + A \times (T - T_{ref}) + B \times (T^2 - {T_{ref}}^2) \quad (3)$$

where T and T_{ref} are the measured temperatures and reference temperature in Kelvin; A and B are constants determined by the inherent properties of the material.

Table 4. Correlation Results of C_p Data for Different Catalytic Materials with Equation (3).

	T_{ref}/K	$C_p(T_{ref})$/(J·kg^{-1}·K^{-1})	A/(J·kg^{-1}·K^{-2})	Estimated Error of A/(J·kg^{-1}·K^{-2})	B/(J·kg^{-1}·K^{-3})	Estimated Error of B/(J·kg^{-1}·K^{-3})	R^2
Activated carbon	392.74	1288.34	2.89	5.57	0.0016	0.0072	0.9992
Al_2O_3	392.73	1003.09	4.37	0.79	−0.0036	0.0010	0.9971
Amberlite IR120, H-form	353.21	1325.63	3.94	0.09			0.9992
H-Beta-25	402.67	1419.67	4.42	0.28			0.9910
H-Beta-38	392.81	1685.38	−19.39	2.47	0.0329	0.0032	0.9981
H-Y−60	372.97	1019.52	0.42	0.35	0.0024	0.0004	0.9998
H-ZSM-5-23	392.77	1194.68	-3.87	0.75	0.0084	0.0010	0.9991
H-ZSM-5-280	392.79	910.64	1.08	0.12			0.9729
SiO_2	392.75	1399.71	−1.94	1.58	0.0337	0.0021	0.9994
TiO_2	402.66	788.29	2.92	0.62	−0.0027	0.0008	0.9944
Zeolite 13X	373.00	1097.44	3.44	1.24	−0.0029	0.0016	0.9907

To compare the fit of the polynomial expression with the experimental results, Athena Visual Studio [29] was used to calculate the errors of the estimated fitting parameters. The obtained error values provide a 0.95 confidence interval.

As can be seen from Table 4, a very satisfactory correlation was obtained for each sample, with a coefficient of determination higher than 97%, although the estimated errors for parameters A and B were not always low. A linear relationship between C_p and T was found for Amberlite IR120, H-Beta-25, and H-ZSM-5-280 in the measured temperature range. Thus, for these materials, the value of B was set to 0.

4. Conclusions

In this study, the evolution of specific heat capacity with temperature was measured for different materials used in the preparation of heterogeneous catalysts. Such a study is important in developing efficient and safe chemical processes.

A commercial Tian–Calvet calorimeter was successfully used, allowing for high accuracy and the possibility of working at high temperatures.

Different families of catalytic materials were tested, including alumina-silicates, aluminum oxide, silicon dioxide, titanium dioxide, activated carbon, and sulfonated resin. It was found that the specific heat capacities increase, to a varying degree, with temperature for these catalytic materials. For example, the C_p of silicon dioxide was more sensitive to a temperature increase than titanium dioxide.

A polynomial correlation for each catalytic material was developed. However, there is not a clear correlation between the Al_2O_3/SiO_2 ratio and the values of C_p. Further investigation is needed to develop stronger relationships, taking into account the effect of catalyst structure and intrinsic properties on the specific heat capacities of these catalytic materials.

Author Contributions: Conceptualization, S.L.; methodology, Y.W.; software, S.L.; validation, X.L.; formal analysis, X.L.; investigation, X.L.; resources, N.K.; writing—original draft preparation, X.L., H.G., and S.L.; writing—review and editing, X.L., H.G., L.E., and S.L.; supervision, H.G., L.E., and S.L. All authors have read and agreed to the published version of the manuscript.

Funding: This study has been done in the framework of Task 2: "Green process: 2nd generation of biomass" of the AMED project. The authors thank the AMED project. The AMED project has been funded with support from the European Union, the European Regional Development Fund (ERDF), and the Regional Council of Normandie. The China Scholarship Council: Cooperation Program with the UTs and INSAs (France) is thanked by the authors. The authors thank the Erasmus program.

Conflicts of Interest: The authors declare no conflicts of interest.

References

1. Talukdar, K.; Helmly, S.; Schulze, M.; Sanchez, D.G.; Handl, M.; Hiesgen, R.; Kraut, J.; Friedrich, K.A. Enveloping of catalyst powder by ionomer for dry spray coating in polymer electrolyte membrane fuel cells. *J. Power Sources* **2019**, *424*, 82–90. [CrossRef]
2. Bossion, A.; Heifferon, K.V.; Meabe, L.; Zivic, N.; Taton, D.; Hedrick, J.L.; Long, T.E.; Sardón, H. Opportunities for organocatalysis in polymer synthesis via step-growth methods. *Prog. Polym. Sci.* **2019**, *90*, 164–210. [CrossRef]
3. Xie, J.; Zhang, X.; Xie, J.; Xu, J.; Pan, L.; Zou, J.-J. Acid-catalyzed rearrangement of tetrahydrotricyclopentadiene for synthesis of high density alkyl-diamondoid fuel. *Fuel* **2019**, *239*, 652–658. [CrossRef]
4. Givirovskiy, G.; Ruuskanen, V.; Ojala, L.S.; Lienemann, M.; Kokkonen, P.; Ahola, J. Electrode material studies and cell voltage characteristics of the in situ water electrolysis performed in a pH-neutral electrolyte in bioelectrochemical systems. *Heliyon* **2019**, *5*, e01690. [CrossRef]
5. Bengyella, L.; Iftikhar, S.; Nawaz, K.; Fonmboh, D.J.; Yekwa, E.L.; Jones, R.C.; Njanu, Y.M.T.; Roy, P. Biotechnological application of endophytic filamentous bipolaris and curvularia: A review on bioeconomy impact. *World J. Microbiol. Biotechnol.* **2019**, *35*, 69. [CrossRef] [PubMed]

6. Sudarsanam, P.; Zhong, R.; Bosch, S.V.D.; Coman, S.M.; Parvulescu, V.I.; Sels, B.F. Functionalised heterogeneous catalysts for sustainable biomass valorisation. *Chem. Soc. Rev.* **2018**, *47*, 8349–8402. [CrossRef]
7. De Clercq, R.; Dusselier, M.; Sels, B.F. Heterogeneous catalysis for bio-based polyester monomers from cellulosic biomass: Advances, challenges and prospects. *Green Chem.* **2017**, *19*, 5012–5040. [CrossRef]
8. Lee, A.; Bennett, J.; Manayil, J.C.; Wilson, K. Heterogeneous catalysis for sustainable biodiesel production via esterification and transesterification. *Chem. Soc. Rev.* **2014**, *43*, 7887–7916. [CrossRef]
9. Zhong, Q.; Dong, X.; Zhao, Y.; Zhang, H.; Wang, J.; Guo, H.; Shen, J.; Gong, M. Thermodynamic properties of (R1234yf + R290): Isochoric pρTx and specific heat capacity c measurements and an equation of state. *J. Chem. Thermodyn.* **2019**, *129*, 36–43. [CrossRef]
10. Ma, B.; Kumar, N.; Kuchibhotla, A.; Banerjee, D. Experimental Measurement of the Effect of Particle Concentration on the Specific Heat Capacity of Silica Nanofluids. In Proceedings of the 2018 17th IEEE Intersociety Conference on Thermal and Thermomechanical Phenomena in Electronic Systems (ITherm), San Diego, CA, USA, 29 May–1 June 2018; pp. 246–251.
11. Lv, S.; Zhao, X.; Liu, Y. Measurements for isobaric specific heat capacity of ethyl fluoride (HFC-161) in liquid and vapor phase. *Fluid Phase Equilibria* **2016**, *427*, 429–437. [CrossRef]
12. Calvin, J.; Asplund, M.; Zhang, Y.; Huang, B.; Woodfield, B.F. Heat capacity and thermodynamic functions of γ-Al2O3. *J. Chem. Thermodyn.* **2017**, *112*, 77–85. [CrossRef]
13. Voskov, A.L.; Voronin, G.F.; Kutsenok, I.B.; Kozin, N.Y. Thermodynamic database of zeolites and new method of their thermodynamic properties evaluation for a wide temperature range. *Calphad* **2019**, *66*, 101623. [CrossRef]
14. O'Neill, M.J. Measurement of Specific Heat Functions by Differential Scanning Calorimetry. *Anal. Chem.* **1966**, *38*, 1331–1336. [CrossRef]
15. Chen, F.; Zhao, T.; Liang, J.; Cao, W.; Jiang, Y.; Xu, X. Specific Heat Capacity Measurements of Frying Oil Using Modulated Differential Scanning Calorimetry. *J. Am. Oil Chem. Soc.* **2019**, *96*, 1011–1018. [CrossRef]
16. Kuprava, A.; Saenko, I.; Fabrichnaya, O. Heat capacity measurement of C14–ZrMn2 and thermodynamic re-assessment of the Mn–Zr system. *Calphad* **2020**, *68*, 101745. [CrossRef]
17. Losada-Pérez, P.; Tripathi, C.S.P.; Leys, J.; Cordoyiannis, G.; Glorieux, C.; Thoen, J. Measurements of Heat Capacity and Enthalpy of Phase Change Materials by Adiabatic Scanning Calorimetry. *Int. J. Thermophys.* **2011**, *32*, 913–924. [CrossRef]
18. Quick, C.; Schawe, J.; Uggowitzer, P.; Pogatscher, S. Measurement of specific heat capacity via fast scanning calorimetry—Accuracy and loss corrections. *Thermochim. Acta* **2019**, *677*, 12–20. [CrossRef]
19. Coulier, Y.; Tremaine, P.R. Standard partial molar heat capacities and enthalpies of formation of aqueous aluminate under hydrothermal conditions from integral heat of solution measurements. *J. Chem. Thermodyn.* **2014**, *78*, 79–92. [CrossRef]
20. Schrödle, S.; Königsberger, E.; May, P.M.; Hefter, G. Heat capacities of aqueous sodium hydroxide/aluminate mixtures and prediction of the solubility constant of boehmite up to 300 °C. *Geochim. Cosmochim. Acta* **2010**, *74*, 2368–2379. [CrossRef]
21. Roháč, V.; Růžička, V.; Růžička, K.; Poledníček, M.; Aim, K.; Jose, J.; Zábranský, M. Recommended vapour and sublimation pressures and related thermal data for chlorobenzenes. *Fluid Phase Equilibria* **1999**, *157*, 121–142. [CrossRef]
22. Reichmann, T.L.; Li, D.; Cupid, D.M. Heat capacities and an updated thermodynamic model for the Li-Sn system. *Phys. Chem. Chem. Phys.* **2018**, *20*, 22856–22866. [CrossRef] [PubMed]
23. Niu, H.; Chen, S.; Jin, S.; Li, B.; Li, X.; Wang, J.; Ma, X.; Bao, F.; Li, L. Preparation, nonisothermal decomposition kinetics, heat capacity, and safety parameters of TKX-50-based PBX. *J. Therm. Anal. Calorim.* **2017**, *131*, 3193–3199. [CrossRef]
24. Wilcock, E.; Rogers, R. A review of the phi factor during runaway conditions. *J. Loss Prev. Process. Ind.* **1997**, *10*, 289–302. [CrossRef]
25. Cai, X.; Aissa, K.A.; Estel, L.; Leveneur, S. Investigation of the Physicochemical Properties for Vegetable Oils and Their Epoxidized and Carbonated Derivatives. *J. Chem. Eng. Data* **2018**, *63*, 1524–1533. [CrossRef]
26. Ariba, H.; Wang, Y.; Devouge-Boyer, C.; Stateva, R.P.; Leveneur, S. Physicochemical Properties for the Reaction Systems: Levulinic Acid, Its Esters, and γ-Valerolactone. *J. Chem. Eng. Data* **2020**, *65*, 3008–3020. [CrossRef]

27. Tan, Z.-C.; Zhang, J.-B.; Shang-He, M. A Low-temperature Automated Adiabatic Calorimeter Heat Capacities of High-purity Graphite and Polystyrene. *J. Therm. Anal. Calorim.* **1999**, *55*, 283–289. [CrossRef]
28. Kowalski, B. Determination of specific heats of some edible oils and fats by differential scanning calorimetry. *J. Therm. Anal. Calorim.* **1988**, *34*, 1321–1326. [CrossRef]
29. Stewart, W.E.; Caracotsios, M. Athena Visual Studio. Available online: www.athenavisual.com (accessed on 10 June 2020).